Two Tabersonine 6,7-Epoxidases Initiate Lochnericine-Derived Alkaloid Biosynthesis in *Catharanthus roseus*[1]

Inês Carqueijeiro,[a] Stephanie Brown,[b] Khoa Chung,[b] Thu-Thuy Dang,[b] Manish Walia,[c] Sébastien Besseau,[a] Thomas Dugé de Bernonville,[a] Audrey Oudin,[a] Arnaud Lanoue,[a] Kevin Billet,[a] Thibaut Munsch,[a] Konstantinos Koudounas,[a] Céline Melin,[a] Charlotte Godon,[d] Bienvenue Razafimandimby,[d] Johan-Owen de Craene,[a] Gaëlle Glévarec,[a] Jillian Marc,[a] Nathalie Giglioli-Guivarc'h,[a] Marc Clastre,[a] Benoit St-Pierre,[a] Nicolas Papon,[d] Rodrigo B. Andrade,[c] Sarah E. O'Connor,[b,2] and Vincent Courdavault[a,2]

[a]Université de Tours, EA2106 Biomolécules et Biotechnologies Végétales, Tours, F-37200, France
[b]John Innes Centre, Department of Biological Chemistry, Norwich NR4 7UH, United Kingdom
[c]Department of Chemistry, Temple University, Philadelphia, Pennsylvania 19122, USA
[d]Université d'Angers, EA3142 Groupe d'Etude des Interactions Hôte-Pathogène, Angers, F-49933, France

ORCID IDs: 0000-0001-9576-5556 (I.C.); 0000-0002-1920-3663 (K.C.); 0000-0002-0028-802X (M.W.); 0000-0002-5518-2580 (S.B.); 0000-0002-2205-2886 (T.D.d.B.); 0000-0002-7377-8177 (A.L.); 0000-0002-6000-6565 (K.K.); 0000-0002-9077-2949 (B.S.); 0000-0002-4554-8323 (R.B.A.); 0000-0001-8902-4532 (V.C.)

Lochnericine is a major monoterpene indole alkaloid (MIA) in the roots of Madagascar periwinkle (*Catharanthus roseus*). Lochnericine is derived from the stereoselective C6,C7-epoxidation of tabersonine and can be metabolized further to generate other complex MIAs. While the enzymes responsible for its downstream modifications have been characterized, those involved in lochnericine biosynthesis remain unknown. By combining gene correlation studies, functional assays, and transient gene inactivation, we identified two highly conserved P450s that efficiently catalyze the epoxidation of tabersonine: tabersonine 6,7-epoxidase isoforms 1 and 2 (TEX1 and TEX2). Both proteins are quite divergent from the previously characterized tabersonine 2,3-epoxidase and are more closely related to tabersonine 16-hydroxylase, involved in vindoline biosynthesis in leaves. Biochemical characterization of TEX1/2 revealed their strict substrate specificity for tabersonine and their inability to epoxidize 19-hydroxytabersonine, indicating that they catalyze the first step in the pathway leading to hörhammericine production. *TEX1* and *TEX2* displayed complementary expression profiles, with *TEX1* expressed mainly in roots and *TEX2* in aerial organs. Our results suggest that *TEX1* and *TEX2* originated from a gene duplication event and later acquired divergent, organ-specific regulatory elements for lochnericine biosynthesis throughout the plant, as supported by the presence of lochnericine in flowers. Finally, through the sequential expression of *TEX1* and up to four other MIA biosynthetic genes in yeast, we reconstituted the 19-acetylhörhammericine biosynthetic pathway and produced tailor-made MIAs by mixing enzymatic modules that are naturally spatially separated in the plant. These results lay the groundwork for the metabolic engineering of tabersonine/lochnericine derivatives of pharmaceutical interest.

Monoterpene indole alkaloids (MIAs) are specialized plant metabolites characterized by potent biological activities, which place these compounds at the heart of defense systems that several Apocynaceae, Rubiaceae, Nyssaceae, and Loganiaceae species have evolved to combat bioaggressors (Luijendijk et al., 1996; Roepke et al., 2010; St-Pierre et al., 2013). For instance, *Catharanthus roseus* (Madagascar periwinkle) accumulates almost 130 distinct MIAs that collectively prevent organ consumption or result in herbivorous intoxication or death upon ingestion (Meisner et al., 1981; van der Heijden et al., 2004; Guirimand et al., 2010; Dugé de Bernonville et al., 2017). These poisonous properties also grant MIAs a prominent position in human pharmacopeia, such as the antimalarial quinine from *Cinchona officinalis*, the antiarrhythmic ajmaline synthesized in *Rauwolfia serpentina*, or the anticancer vinblastine and vincristine produced in *C. roseus*.

For decades, the high value of MIAs has stimulated the elucidation of their biosynthetic pathways, now opening new perspectives toward the engineered production of these compounds in heterologous organisms through gene transfers (Miettinen et al., 2014; Brown et al., 2015; Qu et al., 2015). Besides offering a new type of sourcing for MIAs, these studies resulted in a

[1]This research was supported by "Région Centre-Val de Loire" (France) by funding the CatharSIS program and BioPROPHARM project ARD2020 Biomédicaments. I.C. was supported by a postdoctoral fellowship from Région Centre-Val de Loire. V.C. acknowledges "Le Studium" for a Studium Research Consortium grant. S.E.O. acknowledges an European Research Council grant (311363) and T.-T.D. acknowledges an EMBO long-term fellowship (ALTF 739-2015). R.B.A. and M.W. were supported by the National Science Foundation (CHE-1665145).

[2]Address correspondence to sarah.o'connor@jic.ac.uk or vincent.courdavault@univ-tours.fr.

The author responsible for distribution of materials integral to the findings presented in this article in accordance with the policy described in the Instructions for Authors (www.plantphysiol.org) is: Vincent Courdavault (vincent.courdavault@univ-tours.fr).

S.E.O. and V.C. designed the research; I.C., S.Br., T.-T.D., K.C., T.D.d.B., S.Be., K.B., T.M., A.L., A.O., G.G., M.W., K.K., C.M., C.G., B.R., J.-O.d.C., and J.M. performed research; N.G.G., N.P., M.C., B.S.-P., and R.B.A. analyzed the data; S.E.O and V.C. wrote the article.

www.plantphysiol.org/cgi/doi/10.1104/pp.18.00549

better understanding of their metabolism in the aforementioned plants and especially in *C. roseus*, considered a model nonmodel system (Facchini and De Luca, 2008; Courdavault et al., 2014; Dugé de Bernonville et al., 2015a). Almost all MIAs derive from strictosidine, which undergoes many modifications to generate the different classes of MIAs, including corynanthe (e.g. ajmalicine), iboga (catharanthine), and aspidosperma (tabersonine; O'Connor and Maresh, 2006; Szabó, 2008). Initially, deglucosylation catalyzed by a dedicated glucosidase, strictosidine glucosidase, is required, which is then followed by distinct enzymes that determine the metabolic fluxes toward the synthesis of the different MIA classes (Geerlings et al., 2000). For instance, four medium-chain dehydrogenases/reductases including tetrahydroalstonine synthases and heteroyohimbine synthase have been associated with the formation of the corynanthe MIAs (Stavrinides et al., 2015, 2016). In addition, geissoschizine synthase, geissoschizine oxidase (CYP71D1V1), and four other enzymes have been shown to ensure the synthesis of iboga and aspidosperma MIAs through preakuammicine and stemmadenine formation (Tatsis et al., 2017; Qu et al., 2018). More recently, the two missing enzymes involved in the biosynthesis of both catharanthine and tabersonine have been identified, hence completing the characterization of this highly studied biosynthetic pathway (Caputi et al., 2018).

In *C. roseus*, the metabolism of tabersonine is arguably one of the most interesting, due to the diversity of the resulting MIA end products and because of its organ-dependent organization. In leaves, tabersonine is mostly converted into vindoline, a highly abundant MIA and the precursor of vinblastine/vincristine (Westekemper et al., 1980). This conversion occurs via a seven-step biosynthetic pathway beginning with a C16-hydroxylation catalyzed by tabersonine 16-hydroxylase (T16H2; CYP71D351) and ending with acetylation (St-Pierre et al., 1998; Besseau et al., 2013; Qu et al., 2015). In roots, tabersonine mainly enters the biosynthetic pathway of hörhammericine and echitovenine, two MIAs only differing by epoxidation or reduction at C6,C7 (Fig. 1). Encompassing only four distinct enzymes, the biosynthetic pathway of these MIAs is simpler than that of vindoline but also involves hydroxylation catalyzed by T19H followed by acetylation of the resulting hydroxyl (O'Connor and Maresh, 2006; Giddings et al., 2011). This last reaction was attributed initially to minovincine 19-*O*-acetyltransferase, but recent evidence suggested that acetylation is performed by the tabersonine derivative TAT (Laflamme et al., 2001; Carqueijeiro et al., 2018). Surprisingly, the two enzymes catalyzing modifications at C6,C7 still remain unknown, although 6,7-epoxidation activity has been associated with a cytochrome P450 (Rodriguez et al., 2003). While reduction of the 6,7-alkene gives rise to vincadifformine, epoxidation leads to the synthesis of lochnericine, named after a former name of *C. roseus*, *Lochnera rosea* (Gorman et al., 1959; Nair and Pillay, 1959). Interestingly, lochnericine and its hydroxylated form hörhammericine constitute some of the main MIAs accumulated in *C. roseus* roots and hairy roots, usually explaining why the engineering of vindoline synthesis in hairy roots so far failed due to competition for tabersonine supply (Rodriguez et al., 2003; Peebles et al., 2009; Sun et al., 2017; Carqueijeiro et al., 2018). Furthermore, this lack of characterization also impedes the ordering of the enzymatic steps in the pathway, and the requirement of a specific enzyme sequence still remains an open question.

In our continuing effort to fill the gaps in MIA biosynthetic pathways, we focused on the missing steps of root MIA biosynthesis in *C. roseus*. In this work, we describe the identification of two tabersonine 6,7-epoxidase isoforms displaying marked substrate specificity and a complementary gene expression profile. This gene discovery also allowed engineering of the synthesis of root MIA in yeast by expanding the enzymatic toolbox, which enables controlled modifications of the valuable tabersonine framework.

RESULTS

Identification of Tabersonine 6,7-Epoxidase Candidates through Gene Correlation Analysis

To initiate the identification of tabersonine 6,7-epoxidase candidate genes, we conducted a coexpression analysis of publicly available *C. roseus* RNA sequencing data, including the CDF97 consensus transcriptome and the transcriptomic resource generated through the interaction between *Manduca sexta* and *C. roseus* (Góngora-Castillo et al., 2012; Van Moerkercke et al., 2013; Xiao et al., 2013; Dugé de Bernonville et al., 2015b, 2017). Due to its closest position in the pathway, T19H was used as bait for a Spearman correlation study that allowed the retrieval of 1,526 genes at a 0.6 threshold (Supplemental Table S1). Based on previous experiments potentially associating tabersonine 6,7-epoxidase activity to P450s, we first focused on the 49 sequences encoding members of this large protein family (Rodriguez et al., 2003).

Since all the known P450s metabolizing tabersonine belong to the CYP71 clan, we hypothesized that tabersonine 6,7-epoxidase should be one of the 29 CYP71 members in our gene candidate list (Supplemental Table S1). Within this group, we next focused on the identification of paralogues of T16H2/T16H1 and T19H, two P450s known to modify tabersonine. Interestingly, the T16H paralogues included seven sequences, while only one paralogue of T19H was identified (Fig. 2A). All these candidates displayed an overall gene expression profile similar to T19H, notably characterized by a high expression in hairy roots and methyl jasmonate (MeJA) responsiveness (Fig. 2B), reflecting their high correlation with T19H (Fig. 2C). Sequence alignments also revealed that the seven T16H-like sequences correspond to four distinct genes in the *C. roseus* genome (CRO_T000497, CRO_T013902, CRO_T019212, and

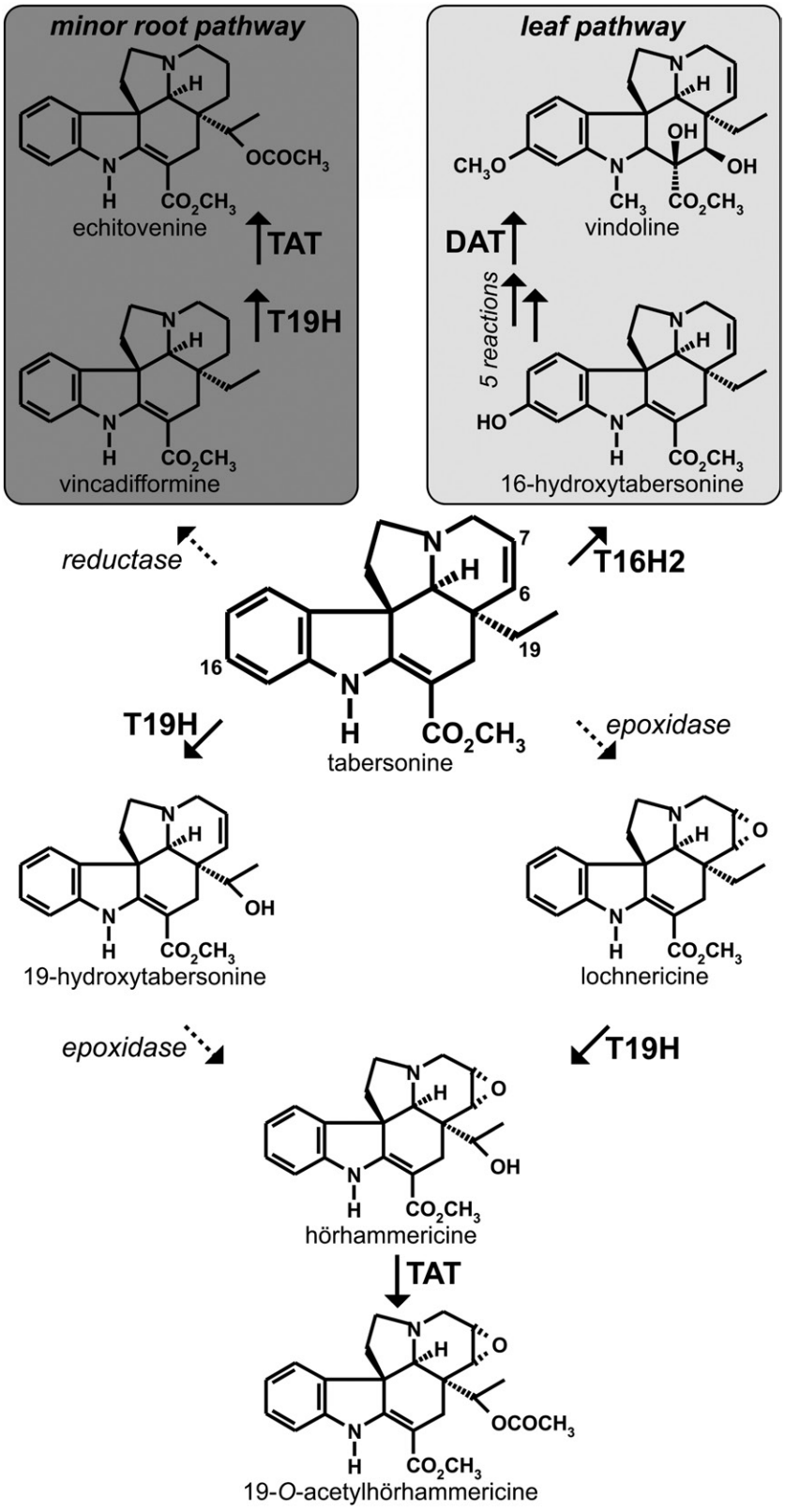

Figure 1. Main routes of tabersonine metabolism in *C. roseus*. Solid and dashed arrows represent characterized and uncharacterized putative reactions, respectively. DAT, Deacetylvindoline 4-*O*-acetyltransferase; TAT, tabersonine derivative 19-*O*-acetyltransferase; T19H, tabersonine 19-hydroxylase. The positions of the carbon atoms subjected to modification are numbered. Note that the convention of carbon numbering shown here is not consistent with IUPAC nomenclature but reflects historical versions of numbering found in the enzymatic literature.

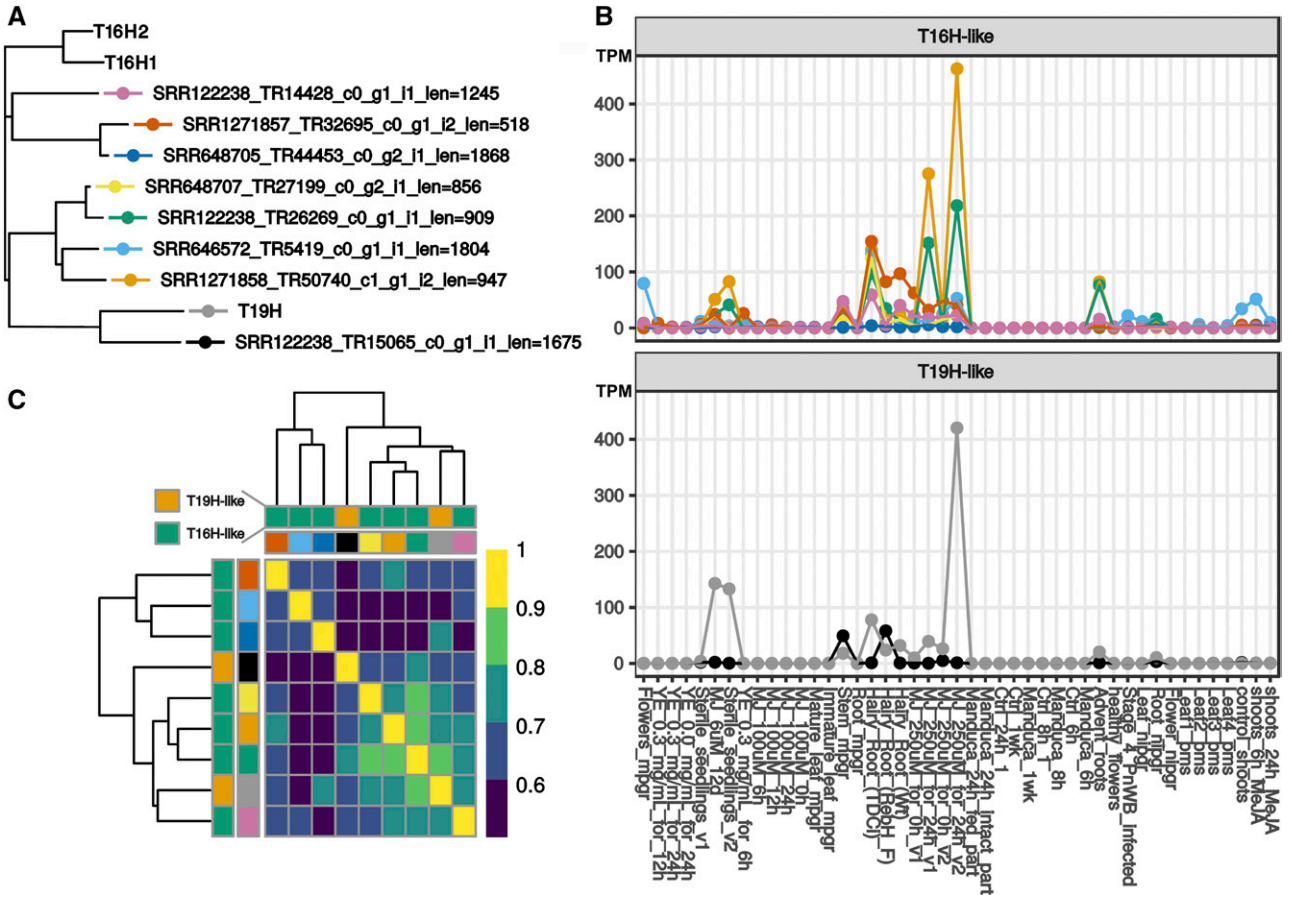

Figure 2. Identification of tabersonine 6,7-epoxidase candidate genes through in silico analysis of T16H- and T19H-related P450s expressed in roots and elicited suspension cells. Best coexpressed genes with T19H (Spearman's $\rho > 0.6$) were obtained from a wide range of experimental conditions. Expression levels were obtained after mapping reads from specific studies on transcripts from the CDF97 assembly. A, Neighbor-joining phylogenetic tree of T16H- and T19H-like P450s in the best coexpressed gene list. T16H1 and T16H2, although expressed mainly in aerial tissues, were added for comparison purposes. B, Expression profiles of T16H- and T19H-like P450s. The color code corresponds to the tags in A. TPM, Transcripts per million. C, Similarity matrix of candidate expression levels. Intensity corresponds to the Spearman's ρ correlation coefficient. Transcripts (inner color code indicates transcript name [see A]; outer color code indicates highest homology) are hierarchically clustered with a Euclidean distance.

CRO_T027852; Supplemental Table S2), exhibiting an overall identity of around 65%, except for CRO_T019212 and CRO_T013902, which were 86% identical (Supplemental Table S3). The T19H-like sequence (CRO_T002923) was 73% identical to T19H. Finally, all five deduced protein sequences bear conserved P450 motifs (Supplemental Fig. S1) and were tested for tabersonine 6,7-epoxidase activity.

CRO_T019212 and CRO_T013902 Encode Two Functional Tabersonine 6,7-Epoxidases

To assay for tabersonine 6,7-epoxidase activity, the coding sequences of the four T16H-like genes (CRO_T000497, CRO_T013902, CRO_T019212, and CRO_T027852) and the T19H-like gene (CRO_T02923) were expressed in yeast by cloning their coding sequences into autoreplicative plasmids bearing inducible promoters. The transformed yeast strains were cultured and induced with Gal before feeding with tabersonine (125 μM) for 24 h, followed by analysis of the resulting products by ultra-performance liquid chromatography-mass spectrometry (UPLC-MS; Fig. 3A).

While the two control yeast strains expressing T16H2 and T19H performed the expected site-specific hydroxylations of tabersonine, no conversion was observed when CRO_T027852, CRO_T000497, and CRO_T002923 were expressed, suggesting that the encoded proteins do no use tabersonine as a starting substrate. By contrast, a substantial consumption of tabersonine was observed when CRO_T019212 and CRO_T013902 were expressed, and this was accompanied by the formation of compounds with a similar mass-to-charge ratio (*m/z*) 353 but eluted at a higher retention time.

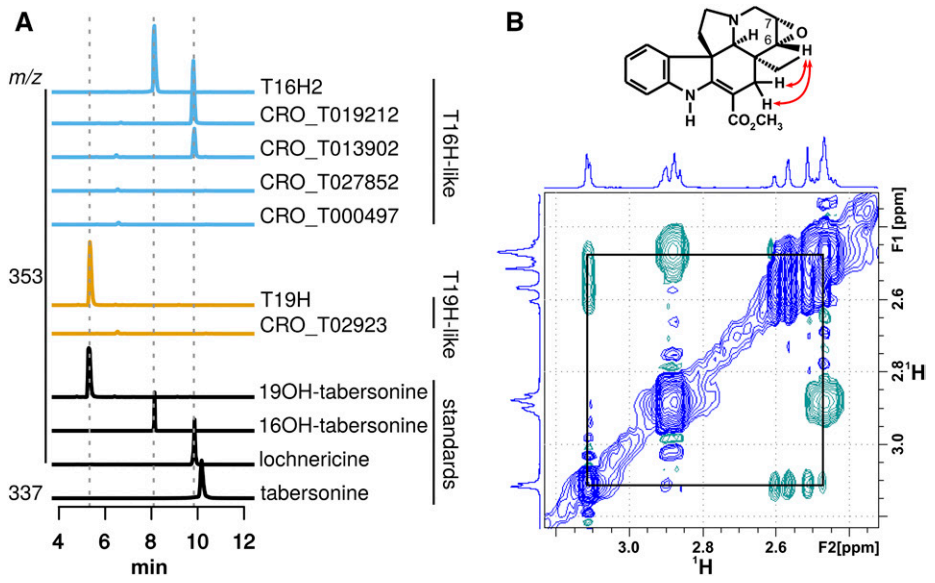

Figure 3. Screening for tabersonine 6,7-epoxidase activity of the selected T16H- and T19H-like P450 candidates. A, Yeast cells expressing T16H2, T16H-like candidates (CRO_T000497, CRO_T013902, CRO_T019212, and CRO_T027852), T19H, or a T19H-like candidate (CRO_T02923) were grown, induced with Gal, and fed with tabersonine (*m/z* 337). The formation of oxygenated derivatives of tabersonine (16-hydroxytabersonine, 19-hydroxytabersonine, or lochnericine) was monitored by LC-MS analyses using selected ion monitoring (*m/z* 353) and comparison with authentic standards. B, The structure of lochnericine was confirmed by NMR analysis (for complete characterization, see Supplemental Figure S3, A and B). The results of NOESY analysis are consistent with the proposed stereochemistry of the epoxide.

Interestingly, these compounds coeluted with lochnericine and displayed similar fragmentation patterns, suggesting that both enzymes synthesized lochnericine (Fig. 3A; Supplemental Fig. S2). To further identify the nature of the modification catalyzed by these proteins, the CRO_T019212 enzymatic product from a milligram-scale reaction was purified by reverse-phase HPLC and analyzed by NMR spectroscopy (Fig. 3B; Supplemental Fig. S3). The proton and carbon chemical shifts of the enzymatic product are very similar to those reported in the literature for tabersonine. However, the H-6 and H-7 protons in this case are strongly shielded relative to the corresponding protons in tabersonine and are found at 3.11 and 3.49 ppm, respectively. Similarly, C6 and C7 also are shielded and are found at 57.2 and 54 ppm, respectively. This suggests that the unsaturation across (C-6)-(C-7) [corresponding to C-15,C-14, respectively in Supplemental Fig. S3] has been lost, and the C-6 and C-7 atoms are likely bonded to oxygen. The *m/z* increase of 16 suggests that only one oxygen atom has been added, resulting in an epoxidation at the C-6,C-7 positions. Moreover, the H-6 proton shows nuclear Overhauser effect (NOE) correlations to both H-4 protons (corresponding to H-17 in Supplemental Fig. S3). This strongly suggests that the epoxide motif is directed upward, as the alternative configuration would place the H-6 proton upward, which would be expected to exhibit only one or possibly no NOE interaction with the H-17 protons. Collectively, these data indicate that this compound might be lochnericine. Comparison with previously reported NMR assignments for lochnericine shows good agreement. This result thus confirms that both CRO_T019212 and CRO_T013902 display tabersonine 6,7-epoxidase activity. As a consequence, CRO_T019212 and CRO_T013902 were named tabersonine 6,7-epoxidase isoform 1 (TEX1 [CYP71D521]; GenBank accession no. MG873080) and isoform 2 (TEX2 [CYP71D347]; GenBank accession no. MG873081), respectively.

TEX1 and TEX2 Display Similar Kinetic Parameters

To gain insight into TEX1 and TEX2 enzymatic specificities, their biochemical properties were analyzed subsequently following purification of the corresponding enriched yeast microsomes. TEX1 and TEX2 microsomes were first incubated with increasing amounts of tabersonine to compare the kinetics parameters of the two enzymes (Table 1; Supplemental Fig. S4). Both enzymes displayed very close apparent K_m and V_{max} values, suggesting that TEX1 and TEX2 exhibit similar catalytic characteristics toward tabersonine. We next analyzed their substrate specificities by assaying TEX1- or TEX2-enriched microsomes against other MIAs and non-MIA compounds such as flavonoids. Ajmalicine, vindoline, and catharanthine, as well as the flavonoids naringenin and kaempferol, were not converted by TEX1 or TEX2, suggesting that both enzymes were specific to the tabersonine backbone of MIAs (Table 1). Furthermore, vincadifformine was not epoxidized by either enzyme, confirming that the presence of unsaturation at the C6,C7 position was required strictly for the formation of an epoxide, as expected for these oxidases. Finally, while 19-hydroxytabersonine still contains the C6-C7 alkene, it was not metabolized by TEX1 or TEX2, thus suggesting that the addition of a hydroxyl close to the C6,C7 position prevents TEX activity. This hypothesis was confirmed in vivo by coexpressing T19H and TEX1 or TEX2 in yeast, which resulted in the formation of 19-hydroxytabersonine, while hörhammericine (19-hydroxylochnericine) was not observed (Supplemental Fig. S5). Altogether, these results suggested that TEX1 and TEX2 are highly specific to tabersonine and do not accept modifications of the C6,C7 functionality.

Table 1. TEX1 and TEX2 substrate specificities

Substrate	TEX1	TEX2
Tabersonine	K_m, 2.08 ± 0.22 μM V_{max}, 0.254 ± 0.006 pmol s^{-1}	K_m, 6.45 ± 0.37 μM V_{max}, 0.108 ± 0.002 pmol s^{-1}
Vincadifformine	–	–
19-Hydroxytabersonine	–	–
Ajmalicine	–	–
Vindoline	–	–
Catharanthine	–	–
Naringenin	–	–
Kaempferol	–	–

TEX1 and TEX2 Are Expressed in an Organ-Dependent Manner

The presence of two TEX isoforms in *C. roseus* prompted us to investigate lochnericine metabolism at the whole-plant level by comparing the amount of lochnericine and derived MIAs with TEX1 and TEX2 gene expression profiles. Both transcript levels were analyzed in the major *C. roseus* organs, revealing opposed expression patterns. While *TEX1* was expressed only in roots, *TEX2* transcripts were detected in all organs except roots, including stem, young and mature leaves, and flowers, in agreement with our transcriptomic analysis (Figs. 2B and 4A). As a control, we showed that *T19H* exhibited an expression pattern restricted to roots and flowers, as reported previously (Carqueijeiro et al., 2018). As such, *TEX1* expression is consistent with that of *T19H* for the high accumulation of lochnericine, hörhammericine, and 19-acetylhörhammericine in roots (Supplemental Table S4). By contrast, no lochnericine or derived MIAs were detected in young/mature leaves that could be linked to the high expression of *TEX2* in these organs. However, the presence of *TEX2* transcripts in flowers may explain the unexpected detection of lochnericine in this reproductive organ. We next compared the absolute expression level of these three genes in wild-type roots, hairy roots, and adventitious roots generated from freshly cut stems of *C. roseus* (Fig. 4B). Interestingly, the differential expression between *TEX1* and *TEX2* was confirmed in roots, with a substantially higher amount of *TEX1* transcripts. By contrast, *TEX2* was associated with high tabersonine 6,7-epoxidase activity in both hairy and adventitious roots, resulting in a marked accumulation of lochnericine (Supplemental Table S5). Again, *T19H* exhibited dramatically lower expression, in agreement with the low amounts of hörhammericine and 19-acetylhörhammericine (Supplemental Table S5). Finally, we confirmed the high MeJA responsiveness of both *TEX1* and *TEX2* (500- and 4,500-fold induction, respectively), as suggested by transcriptomics (Figs. 2B and 4C). In agreement with the presence of putative transmembrane helices at their N termini, the expression of TEX1 and TEX2 fused to yellow fluorescent protein (YFP) suggested that both enzymes are anchored to the endoplasmic reticulum, as observed previously for other P450s that metabolize tabersonine (Fig. 4, D–K; Supplemental Fig. S6; Besseau et al., 2013; Carqueijeiro et al., 2018).

Silencing of TEX1 Negatively Impacts Lochnericine Accumulation in Roots

To investigate the role of TEXs in lochnericine biosynthesis in planta, we applied a transient silencing approach through virus-induced gene silencing. Although roots are less prone to silencing, we targeted *TEX1* given the high amount of lochnericine accumulated in this organ type, thus enabling efficient analysis of the metabolic consequences of gene silencing. To conduct this study, young plantlets were transformed with a *TEX1* silencing construct (viTEX1) or an empty vector (EV) as a control. These transformed plantlets exhibited strongly altered root phenotypes such as reduced growth, which might result from a virus or *Agrobacterium tumefaciens* propagation (Fig. 5A), as reported in a previous study (Weaver et al., 2014). However, we measured a substantial decrease of *TEX1* expression in viTEX1 plants as compared with EV (Fig. 5B). Such gene silencing was accompanied by a decrease of lochnericine production and, conversely, by an increase of tabersonine accumulation in viTEX1 plants (Fig. 5C). This result thus confirms that TEX1 is involved in the biosynthesis of lochnericine in *C. roseus* plants.

Metabolic Engineering of the Biosynthesis of 6,7-Oxygenated Tabersonine Derivatives in Yeast

Due to the highly valuable properties of some tabersonine derivatives exhibiting a C6,C7-epoxide, we next evaluated the possibility of reconstituting a tabersonine bioconverting system by coexpressing several tabersonine-metabolizing enzymes together in yeast (Kojima and Umezawa, 2006; Lim et al., 2008). We first chose to reconstitute the 19-acetylhörhammericine biosynthetic pathway by coexpressing TEX1, T19H, and TAT.

Due to the high substrate specificity of TEX1, which is not capable of epoxidizing 19-hydroxytabersonine, TEX1 is required to act before the subsequent reactions catalyzed by T19H and TAT (Table 1; Supplemental Fig. S5). Such sequential conversions were achieved by cloning the TEX1 coding sequence under the control of a constitutive promoter (phosphoglycerate kinase1 in pXP218), while T19H and TAT were controlled by

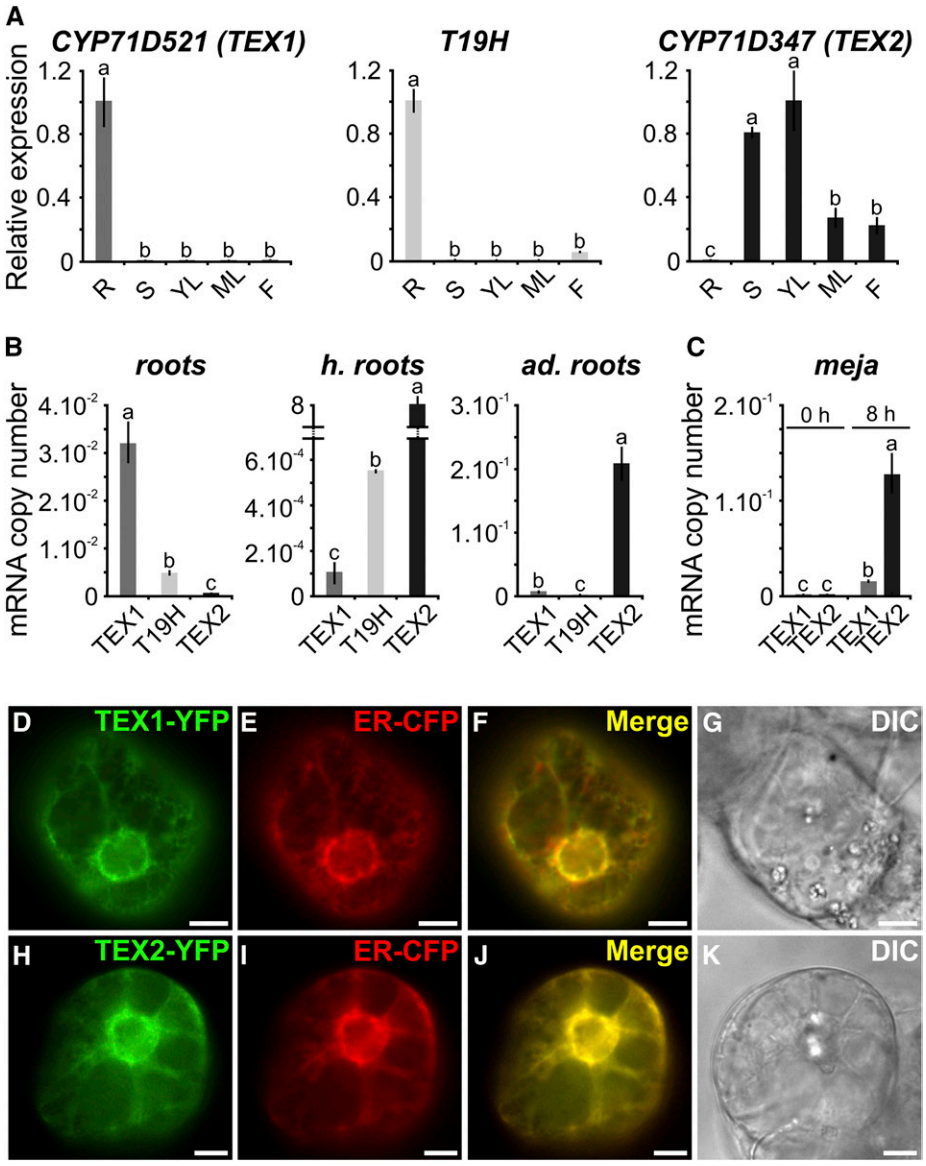

Figure 4. Transcript distribution and subcellular protein localization of TEX1 and TEX2. A, *TEX1* is expressed exclusively in roots (R), while *TEX2* is expressed in all aerial organs examined, including stems (S), young leaves (YL), mature leaves (ML), and flowers (F). *T19H* displays a mixed expression profile, with transcripts detected in roots and flowers. B, *TEX1*, *TEX2*, and *T19H* transcript copy numbers (expressed as reference gene ratio) in roots, hairy (h.) roots, and adventitious (ad.) roots showing a lowest *T19H* transcript level compared with *TEX1* or *TEX2*. C, Both *TEX1* and *TEX2* display MeJA-inducible expression. Relative and absolute transcript quantifications of each gene were determined by reverse transcription-quantitative PCR (qPCR) analyses performed on RNA extracted from various *C. roseus* organs. Data represent means ± SE of three technical replicates performed individually on six samples of each organ type. Different letters indicate different statistical classes ($P < 0.05$; Tukey's honest significant differences). D to K, TEX1 and TEX2 are localized to the endoplasmic reticulum (ER). *C. roseus* cells were transiently cotransformed with plasmids expressing TEX1-YFP (D) or TEX2-YFP (H) with an ER-CFP marker (E and I). Colocalization of the two fluorescence signals appears on the merged images (F and J). Cell morphology (G and K) was observed with differential interference contrast (DIC). Bars = 10 μm.

Gal-inducible promoters (GAL1/10 in pYEDP60 and pESC-Trp, respectively). Using a yeast strain transformed with these three plasmids, a first 24 h of growth in glycerol-enriched medium allowed an almost complete conversion of tabersonine into lochnericine (Fig. 6). The subsequent induction of T19H and TAT expression through Gal addition resulted in the hydroxylation and acetylation of lochnericine, leading to the synthesis of 19-acetylhörhammericine (Fig. 6). Interestingly, almost all synthesized MIAs were excreted to the yeast culture medium. The production of the final compound reached between 12% and 25% of the tabersonine substrate, similar to previous observations for such bioconversion (Carqueijeiro et al., 2018). This three-enzyme coexpressed system thus allows a complete reconstitution of the 19-acetylhörhammericine biosynthetic pathway from tabersonine and opens new opportunities toward the tailor-made synthesis of tabersonine-derived MIAs.

To illustrate the potential of such an approach, we next added a supplemental decoration capacity by introducing tabersonine C16 modifications through the simultaneous expression of T16H2 and 16-hydroxytabersonine 16-*O*-methyltransferase (16OMT), two enzymes involved in vindoline biosynthesis (Levac et al., 2008; Besseau et al., 2013) that are not naturally involved in these root-specific pathways. Both coding sequences were cloned under the control of GAL1/10-inducible promoters in pESC-Leu, and the resulting plasmid was cotransformed with the TEX1-expressing plasmid to generate a yeast strain coexpressing TEX1, T16H2, and 16OMT. Using the sequential culture process described above, we noted that lochnericine resulting from TEX1 constitutive expression was converted further into a compound exhibiting an *m/z* 383 consistent with

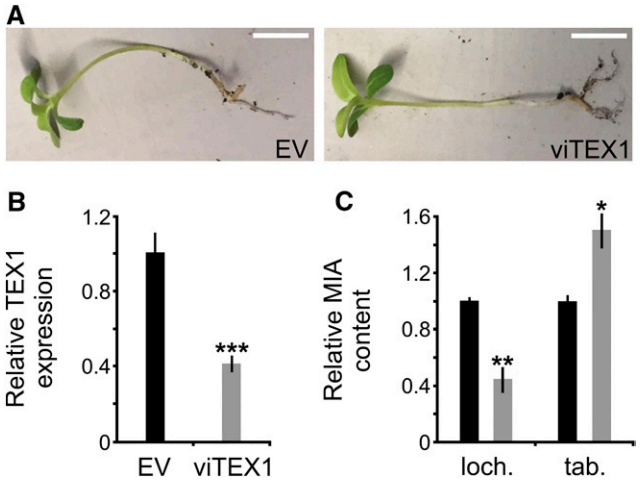

Figure 5. Silencing of *TEX1* decreases lochnericine accumulation in *C. roseus* roots. A, Phenotypes of plantlets transformed with empty pTRV2 vector (EV) or the TEX1-silencing construct (viTEX1). Bars = 1 cm. B, Relative expression of *TEX1* in roots of EV (black bar) and viTEX1 (gray bar) measured by qPCR. C, Relative mean lochnericine (loch.) and tabersonine (tab.) contents in roots of EV (black bar) and viTEX1 (gray bar) transformed plants. Data represent means ± SE of three technical replicates performed on four plants transformed with EV or viTEX1. Asterisks denote statistical significance (*, $P < 0.05$; **, $P < 0.005$; and ***, $P < 0.001$, by Student's *t* test).

lochnerinine (16-methoxylochnericine) after T16H2- and 16OMT-induced expression (Supplemental Fig. S7). This result suggested that these three enzymes can successively metabolize tabersonine into this rare MIA in yeast. As a consequence, we finally coexpressed TEX1, T19H, TAT, T16H2, and 16OMT in the same yeast cells. After feeding with tabersonine and sequential gene expression, we observed that this yeast strain produced a compound with an *m/z* 411 consistent with 16-methoxy-19-acetylhörhammericine as a result of the five-step enzymatic sequence (Supplemental Fig. S7). While we succeeded previously in the synthesis of this compound through the bioconversion of hörhammericine (Carqueijeiro et al., 2018), the achievement of this production from tabersonine constitutes a marked improvement, since tabersonine can be obtained in a higher yield in plants relative to hörhammericine (Koroch et al., 2009). Furthermore, the development of such a yeast strain further enriches the toolbox dedicated to the metabolic engineering of MIAs and the capacity to achieve a tailor-made synthesis of this compound type.

DISCUSSION

While lochnericine constitutes one of the main MIAs from *C. roseus* roots, the key enzyme responsible for the epoxide structure has remained unknown for several decades. In this work, we describe the identification of two isoforms of tabersonine 6,7-epoxidase named TEX1 and TEX2 and, thus, completed the main biosynthetic route of tabersonine derivatives in *C. roseus* roots.

By combining gene expression correlation analyses and yeast assays, we identified two enzymes (TEX1 and TEX2) catalyzing the synthesis of a similar product. NMR characterization revealed the compound to be lochnericine (Figs. 2 and 3). Additional evidence of their function in planta was obtained through TEX1 gene inactivation, resulting in a decrease of lochnericine accumulation in *C. roseus* roots (Fig. 5, B and C). While TEX1 (CYP71D521) and TEX2 (CYP71D347) both belong to the CYP71 clan, we noted that their degree of identity was higher to T16H compared with T19H, even though T16H acts on the indole moiety of tabersonine. On the other hand, TEX1/2 and T19H both act on the terpenoid backbone of tabersonine (Supplemental Fig. S1; Supplemental Table S3). Surprisingly, identity was even lower (46%) to the only other MIA biosynthetic enzyme known so far to catalyze epoxidation, tabersonine 3-oxidase (T3O; Kellner et al., 2015; Qu et al., 2015), suggesting that TEX1 and TEX2 may originate from an ancestor closer to T16H or that selection pressure was lower on T3O. This finding thus reinforces the importance of diversification of the CYP71 clan for the biosynthesis of poststrictosidine MIAs, as observed in *C. roseus* (Schröder et al., 1999; Besseau et al., 2013; Kellner et al., 2015; Tatsis et al., 2017). Interestingly, as suggested by locus tagging, *TEX1* (CRO_T019212) and *TEX2* (CRO_T013902) occupy distant positions in the *C. roseus* genome, implying that a duplication event was followed by gene translocation along with recruitment of the two gene copies into distinct lochnericine synthesis-responsive mechanisms.

At the biochemical level, both isoforms display similar kinetic parameters and substrate specificities (Table 1; Supplemental Fig. S4). Besides being specific to the tabersonine backbone, TEX1 and TEX2 require the presence of the C6,C7-alkene to perform epoxidation, as revealed by the lack of vincadifformine conversion. This requirement is based on their catalytic mechanism, as described for other epoxidases such as zeaxanthin epoxidase (Marin et al., 1996) and squalene epoxidase (Rasbery et al., 2007). Surprisingly, neither TEX1 nor TEX2 accepts 19-hydroxytabersonine as a substrate, in contrast with T19H, which can hydroxylate both tabersonine and lochnericine (Table 1; Giddings et al., 2011). This substrate specificity thus suggests that TEX1 and TEX2 are highly sensitive to the environment proximal to the C6,C7 double bond, and we can hypothesize that the addition of a hydroxyl at C19 increases steric hindrance and/or local polarity, altering substrate recognition. As a physiological consequence, this specificity directs the reaction order in the lochnericine/hörhammericine biosynthetic pathway that strictly requires that 6,7-epoxidation proceeds before 19-hydroxylation, to yield lochnericine and then hörhammericine. This hypothesis is further supported by the high amount of lochnericine measured in roots versus the very low accumulation of 19-hydroxytabersonine (Supplemental

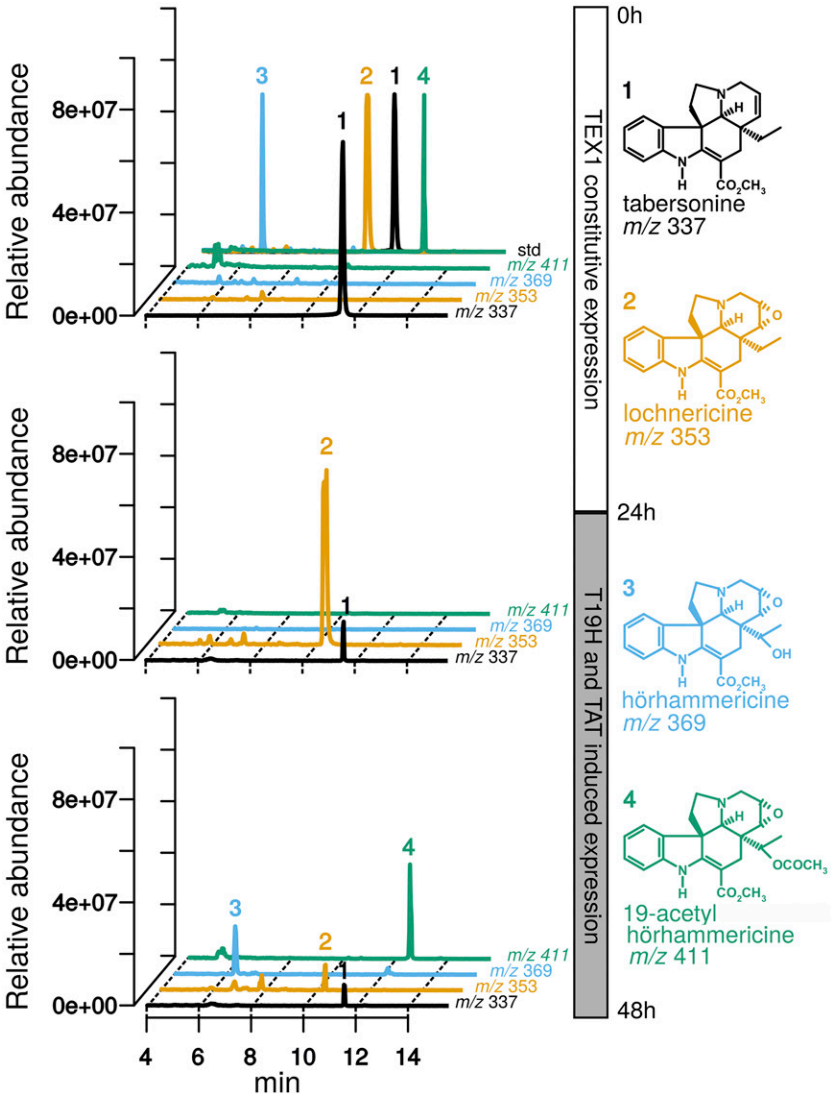

Figure 6. Reconstitution of the tabersonine-to-19-acetylhörhammericine biosynthetic pathway in yeast. Yeast expressing TEX1 and T19H/TAT under the control of constitutive and Gal-inducible promoters, respectively, were fed with tabersonine (1) and grown during 24 h in the absence of Gal to specifically allow TEX1 activity, leading to lochnericine (2) production. Induction of T19H and TAT expression via Gal addition then resulted in the conversion of lochnericine into hörhammericine (3) and 19-acetylhörhammericine (4) during the subsequent 24-h growth period. The three chromatograms successively highlight the MIA composition (expressed as relative peak areas) in the yeast culture medium at 0, 24, and 48 h after tabersonine feeding. std, Standards.

Table S4; Carqueijeiro et al., 2018). Interestingly, T19H displays a high affinity and catalytic efficiency for tabersonine (K_m of 300 nM; Giddings et al., 2011). While comparing catalytic properties remains quite difficult between different studies, especially for P450s that are not all quantifiable by carbon monoxide spectrum (e.g. TEX1 and TEX2), this noticeable difference, as well as our observations in yeast (Supplemental Fig. S5), argue for a higher catalytic activity of T19H versus TEX1 or TEX2 that should favor the formation of 19-hydroxy-tabersonine in vivo at the expense of lochnericine. However, the higher expression levels of *TEX1/TEX2* than *T19H* may have a stronger impact than the higher affinity of T19H toward tabersonine, leading to a preferential flux of tabersonine toward the biosynthesis of lochnericine (Fig. 4B). One can also hypothesize that a multitissue organization may orchestrate this preferential synthesis, with *TEX* and *T19H* expressed in distinct root tissues, as observed in leaf for vindoline synthesis (Courdavault et al., 2014).

As already depicted for other MIA biosynthetic genes in *C. roseus* (Dugé de Bernonville et al., 2015b; Stavrinides et al., 2015, 2016), more than one gene copy governs lochnericine synthesis in planta. Interestingly, while tabersonine 6,7-epoxidase activity has been detected only in roots (Rodriguez et al., 2003), we showed that *TEX1* and *TEX2* display complementary gene expression profiles, with *TEX1* in roots and *TEX2* in aerial organs and hairy/adventitious roots (Fig. 4, A–C). This contrasting distribution pattern resembles that of T16H1 and T16H2 isoforms in flowers and leaves of *C. roseus* (Besseau et al., 2013). In this study, the observed discrepancies between RNA sequencing and qPCR expression profiles may originate from the high degree of identity between both genes, resulting in chimeric transcript reconstitution or spurious read attribution that caused a mix of *TEX1* and *TEX2* expression patterns in the transcriptomic analysis (Figs. 2B and 4A). Based on the qPCR results, we suggest that the expression of *TEX1* is mainly responsible for lochnericine synthesis in roots, while *TEX2* is responsible for lochnericine

production in aerial organs. This hypothesis is supported by the accumulation of lochnericine in *C. roseus* flowers and by the coexpression of *T19H* in this organ (Fig. 4A; Supplemental Table S4). However, we never observed lochnericine or its root-type derivatives in leaves, despite the high TEX2 expression. This may be explained by the presence of other biosynthetic enzymes in these organs that also can metabolize MIAs with a tabersonine backbone, such as T16H2 or other yet unknown enzymes, resulting in the formation of uncharacterized MIAs. For instance, although we did not measure it in this work, lochnerinine (16-methoxylochnericine) and hörhammerinine (16-methoxyhörhammericine) already have been detected in *C. roseus* and *Catharanthus lanceus* leaves, respectively (Maloney et al., 1965; Farnsworth et al., 1968). Interestingly, *TEX2* promoter sequence analysis revealed the presence of a CTCGAG motif that is known to bind phytochrome-interacting factors (Supplemental Fig. S8). By interacting with phytochromes, these transcription factors participate in many light responses that may explain the expression of TEX2 in *C. roseus* aerial organs (Leivar and Quail, 2011). Besides expression in these organs, TEX2 also displays high expression in adventitious and hairy roots in our growth conditions (Fig. 4B). This high expression, in turn, may cause the high accumulation of lochnericine/hörhammericine in hairy roots, making TEX2 a preferential target in inactivation strategies aimed at producing hairy roots with reoriented MIA metabolism (Supplemental Table S5; Sun et al., 2017). Also, the MeJA inducibility of both *TEX1* and *TEX2* is supported by the increased synthesis of lochnericine upon MeJA treatment and may reflect TEX involvement in plant defense mechanisms (Peebles et al., 2009).

Finally, the identification of TEX1/TEX2 expands the toolbox dedicated to the metabolic engineering of MIAs in yeast that we developed recently (Carqueijeiro et al., 2018). First, by ensuring an efficient epoxidation of tabersonine (Fig. 6), it allows a controlled and easy synthesis of lochnericine, given the abundant sourcing of tabersonine (Koroch et al., 2009). Lochnericine displays cytotoxic properties against human leukemia cells in combination with other MIAs. Therefore, yeast bioproduction constitutes an alternative sourcing for this compound that may facilitate future uses (Fernández-Pérez et al., 2013). Second, it enables the full reconstitution of the 19-acetylhörhammericine pathway up to the synthesis of uncommon MIAs, such as 16-methoxy-19-acetylhörhammericine, by mixing enzymatic modules from roots (T19H and TAT) and leaves (T16H2 and 16OMT; Fig. 6; Supplemental Fig. S7). While such an association also has been reported in *C. roseus* hairy roots through T16H and 16OMT overexpression, it did not enable full control of the synthesis of the final MIAs and was limited to the production of some intermediates such as lochnerinine (Sun et al., 2018). By contrast, in our yeast system, the sequential expression of genes enabled a rationalized enzyme activity, resulting in a streamlined reorientation of the metabolic flux up to the expected MIA. Since the yield of these conversions remained low, further optimizations will be required to control the relative yields. However, this study offers concrete opportunities toward the production of tabersonine analogs. Tabersonine is a lead anti-Alzheimer compound, and structural variants may have improved properties for amyloid β-fibril disruption (Kai et al., 2015).

In conclusion, we identified two P450s, TEX1 and TEX2, catalyzing the epoxidation of tabersonine to produce lochnericine in an organ-dependent manner, thus completing one MIA biosynthetic branch of *C. roseus* roots. Their high substrate specificity sheds light on the biosynthetic order governing the synthesis of 19-acetylhörhammericine, placing TEX1/TEX2 as obligatory starting enzymes of this pathway. Such identification also broadens our capacity to achieve MIA production in heterologous organisms such as yeast, allowing for a tailor-made synthesis of MIA resulting from combining distinct enzymatic modules. Expanding the combinatorial synthesis of MIAs and improving the metabolic engineering of tabersonine derivatives is important, given the pharmaceutical potential of highly oxidized congeners of tabersonine, including jerantinine, pachyisphine, taberhanine, melodinine, or conophylline, whose production and access could be facilitated (Kam et al., 2003; Kojima and Umezawa, 2006; Lim et al., 2008; Feng et al., 2010).

MATERIALS AND METHODS

Chemicals

Tabersonine was purchased from ChromaDex, while lochnericine and hörhammericine were purified from *Catharanthus roseus* hairy roots according to Giddings et al. (2011). Vincadifformine was prepared by the hydrogenation of tabersonine as described by Zhao and Andrade (2013).

Transcriptomic Analysis and Identification of Tabersonine 6,7-Epoxidase Candidate Genes

The CDF97 reference transcriptome (Dugé de Bernonville et al., 2015b) was used to obtain expression levels from a wide range of experimental conditions (Supplemental Table S1). Raw reads were obtained from the National Center for Biotechnology Information Short Read Archive with the SRA Toolkit version 2.6.2 and quasimapped onto reference transcripts with Salmon version 0.8.2 to quantify transcript abundance (Patro et al., 2017). Spearman nonparametric correlations were calculated with R version 3.4.1 (R Development Core Team, 2013). Among transcripts that correlated best with T19H, P450s were identified according to reference transcript annotations performed by BlastX (Blast+ version 2.2.29; Camacho et al., 2009) against Uniprot and by hmmscan version 3.1 (Eddy, 2011) against PfamA. Candidates were clustered according to either their sequence similarities with a neighbor-joining tree in ClustalO version 1.2.2 (Sievers et al., 2011) or their expression levels with a Euclidean distance together with a Ward clustering algorithm in R.

Heterologous Expression of Tabersonine 6,7-Epoxidase Candidate Genes in Yeast

Full-length open-reading frames of CRO_T000497, CRO_T013902, CRO_T027852, CRO_T002923, T16H2, and T19H were amplified using dedicated primers (Supplemental Table S6) that have been designed to introduce *Bam*HI or *Spe*I restriction sites at their extremities, allowing cloning into the pESC-His plasmid. Recombinant plasmids were independently used to transform the

Saccharomyces cerevisiae strain WAT11 expressing the Arabidopsis (*Arabidopsis thaliana*) NADPH P450 reductase1 (Pompon et al., 1996). Transformed yeasts were grown in 4 mL of CSM medium (0.67% (w/v) yeast nitrogen base, 2% (w/v) dextrose, and 0.05% (w/v) dropout mix without His) until reaching the stationary phase of culture and prior to being harvested by centrifugation. Protein expression was induced by cultivating the harvested yeast in 10 mL of YPGal medium (2% bacto peptone, 1% yeast extract, and 2% Gal) for 6 h as described by Parage et al. (2016).

Tabersonine 6,7-Epoxidase Functional Assay and Large-Scale Product Synthesis

Functional assays of tabersonine 6,7-epoxidase activity were conducted by feeding 175 µL of Gal-induced recombinant yeast strains with tabersonine (125 µM) during 16 h at 30°C under continuous shaking. Reactions were centrifuged (10 min at 5,000*g*), and supernatants were collected before adding three methanol volumes. Following homogenization with vortexing, reactions were centrifuged (15 min at 25,000*g*) before subsequent UPLC-MS analysis. For large-scale product synthesis of CRO_T019212 (TEX1), 100 mL of the TEX1-expressing yeast strain was grown, induced, and fed with 3.4 mg of tabersonine for 24 h at 30°C. A prepurification was conducted according to Carqueijeiro et al. (2018) before a final purification performed by preparative HPLC on a Thermo Dionex Ultimate 3000 chromatography apparatus using a Phenomenex Luna C18 (5 µm, 30 × 250 mm) column. The solvents used were 0.01% acetic acid (solvent A) and acetonitrile (solvent B). A linear gradient from 5% B to 50% B over 25 min was used to separate the alkaloids. Chromatography was performed at a flow rate of 30 mL min^{-1} and monitored with a UV detector at 254 nm. Fractions (30 mL) were collected and pooled and then characterized by NMR.

Microsome Purification and Steady-State Enzyme Kinetics

Microsomes enriched with TEX1 or TEX2 were isolated using the high-density procedure as described by Heitz et al. (2012). After total microsomal protein quantification, TEX1 and TEX2 activity assays were conducted in a final volume of 50 µL containing 100 mM Tris-HCl, pH 8, 4 mM DTT, 500 µM NADPH, various amounts of substrates, and 37 µg of microsomal proteins. Reactions were initiated by adding NADPH to the reaction mixtures at 30°C and stopped by the addition of methanol (50 µL) before UPLC-MS analysis. Additional assays performed without NADPH or with microsomes from yeast harboring the empty expression vector were used as controls. For kinetic parameter determination, tabersonine was used at concentrations ranging from 0.5 to 50 µM. Nonlinear regression (SigmaPlot 12.0) was used to determine K_m and V_{max} using the Michaelis-Menten equation. For substrate specificity evaluation, reactions were carried out at 30°C during 30 min with vincadifformine, 19-hydroxytabersonine, ajmalicine, vindoline, catharanthine, naringenin, or kaempferol at 100 µM. For UPLC-MS analyses, reactions were stopped by adding 1 volume of methanol. Solutions were vortexed and centrifuged for 10 min at 16,000*g* before collecting 5 µL of the supernatant for injection.

UPLC-MS Analyses

UPLC-MS analyses were conducted using equipment and conditions described by Parage et al. (2016). Data collection was carried in selected ion monitoring mode for the following compounds: tabersonine, *m/z* 337, retention time (RT) = 10.9 min in Figure 3 and 11.52 min in Figure 6 and Supplemental Figures S5 and S7; catharanthine, *m/z* 337, RT = 9.71 min; 16-hydroxytabersonine, *m/z* 353, RT = 8 min; 19-hydroxytabersonine, *m/z* 353, RT = 5.65 min in Figure 3 and 7.8 min in Supplemental Figure S5; ajmalicine, *m/z* 353, RT = 9.76; lochnericine, *m/z* 353, RT = 10.03 min in Figure 3 and 10.4 min in Figure 6 and Supplemental Figures S5 and S7; vincadifformine, *m/z* 339, RT = 11.4 min; 16-methoxytabersonine, *m/z* 367, RT = 12.3 min; 16-hydroxylochnericine, *m/z* 369, RT = 6.4 min; hörhammericine, *m/z* 369, RT = 6.3 min; 16-methoxylochnericine, *m/z* 383, RT = 11.2 min; 16-hydroxyhörchammericine, *m/z* 385, RT = 4.11 min; 16-methoxyhörhammericine, *m/z* 399, RT = 10.7 min; 19-acetylhörhammericine, *m/z* 411, RT = 12.46 min; 16-methoxy 19-acetylhörhammericine, *m/z* 441, RT = 11.25 min; vindoline, *m/z* 457, RT = 12.62 min; 16-methoxylochnericine, *m/z* 383, RT = 11.2 min; 16-methoxy-19-acetylhörhammericine, *m/z* 441, RT = 11.2 min; naringenin, *m/z* 271 (negative electrospray charge (es-)), RT = 12.28 min; and kaempferol, *m/z* 285 (es-), RT = 13.12 min. Discrepancies in RT values resulted from conducting analyses on distinct UPLC devices.

NMR Spectroscopy

NMR spectra (1D and 2D NMR) were acquired using a Bruker Avance III 400 NMR spectrometer equipped with a BBFO plus 5-mm probe. TopSpin version 3.2 was used for analysis. The residual ^{1}H- and ^{13}C-NMR signals of $CDCl_3$ (δ 7.26 and 77.16, respectively) were used for calibration. Proton spectrum used 64 scans; COSY, eight scans; NOESY, eight scans; TOCSY, eight scans; HSQC, 16 scans; HMBC, 64 scans.

Gene Expression Measurement (Reverse Transcription-PCR)

The expression levels of *TEX1*, *TEX2*, and *T19H* were analyzed by quantitative reverse transcription-PCR according to Carqueijeiro et al. (2018) and Liscombe and O'Connor (2011) using primers compiled in Supplemental Table S6, *RPS9* and *EF1α* as endogenous reference genes, and retrotranscribed RNAs from different *C. roseus* organs (including roots, stems, young and mature leaves, flowers [cv Apricot Sunstorm], adventitious roots, and hairy roots).

Subcellular Localization Studies

Subcellular localizations of TEX1 and TEX2 were studied by creating fluorescent fusion proteins using the pSCA-cassette YFPi plasmid (Guirimand et al., 2009). The full-length open reading frames of enzymes were amplified using specific primer couples (Supplemental Table S6), which were designed to introduce the *Spe*I restriction site at both cDNA extremities. PCR products were cloned at the 5′ end of the YFP coding sequence to generate the TEX1-YFP and TEX2-YFP fusion proteins and to maintain the functionality of the predicted N-terminal transmembrane helices (Supplemental Fig. S6). The resulting plasmids were used for transient transformations in combination with plasmids expressing the endoplasmic reticulum-CFR marker (Nelson et al., 2007). Transient transformation of *C. roseus* cells by particle bombardment and fluorescence imaging were performed following the procedures described previously (Foureau et al., 2016). Briefly, *C. roseus* plated cells were bombarded with DNA-coated gold particles (1 µm) and a 1,100-p.s.i. rupture disc at a stopping-screen-to-target distance of 6 cm, using the Bio-Rad PDS1000/He delivery system. Cells were cultivated for 16 to 38 h before being harvested and observed. The subcellular localization was determined using an Olympus BX-51 epifluorescence microscope equipped with an Olympus DP-71 digital camera and a combination of YFP and CFP filters. The pattern of localization presented in this work is representative of approximately 50 observed cells.

TEX1 Invalidation through Virus-Induced Gene Silencing

A TEX1-silencing fragment was amplified using primers viTEX1for and viTEX1rev (Supplemental Table S6) to generate a 381-bp cDNA displaying low identity with other *C. roseus* P450s except for TEX2 (87% identity). This high identity and the presence of strictly identical 21-mer short sequences potentially results in the cross-silencing of both genes. After cloning of this amplicon into the pTRV2 vector, gene silencing was achieved in *C. roseus* plantlets according to the procedure of Sung et al. (2014). Around 200 plantlets were transformed with this silencing construct and empty pTRV2 vector. As a control, additional transformations were performed to silence the phytoene desaturase gene. Five weeks posttransformation, roots were collected, frozen in liquid nitrogen, ground using a mixer mill (Retsch MM400), and subjected to qPCR and UPLC-MS analyses to measure gene expression and MIA content. Due to the recalcitrance of gene silencing in roots, only four transformed plants (expressing viral RNA) were identified for each construct.

Metabolic Engineering of MIA Synthesis in Yeast

The bioconversion of tabersonine into 19-acetylhöhammericine was achieved through the coexpression of TEX1, T19H, and TAT in yeast. For this assay, TEX1 was cloned into pXP218 under the control of the constitutive phosphoglycerate kinase1 promoter, while T19H and TAT were cloned in the *Bam*HI and *Spe*I restriction sites of pYE-DP60 and pESC-Trp, respectively, and T16H2 and 16OMT in the *Spe*I and *Bam*HI restriction sites of pESC-Leu under the control of the GAL1/10 promoter, after amplification of their coding sequences with primers compiled in Supplemental Table S6. Recombinant plasmids were transformed into the WAT11 yeast strain to express the combination of three enzymes (pX218-TEX1, pYeDP60-T19H, and pESC-Trp-TAT to

coexpress TEX1, T19H, and TAT; pXP218-TEX1, pESC-Leu-T16H2/16OMT to coexpress TEX1, T16H2, and 16OMT) or the combination of the five enzymes (pXP218-TEX1, pESC-Leu-T16H2/16OMT, pYeDP60-T19H, and pESC-Trp-TAT). Transformed yeasts were selected onto CSM medium (0.67% yeast nitrogen base, 2% dextrose, and 0.05% dropout mix without adenine for pYE-DP60 plasmid selection, uracil for pXP218 selection, Trp for pESC-TRP selection, and Leu for pESC-Leu selection) and grown in 10 mL of YPD at 28°C for 16 h. Cells were then pelleted by centrifugation (3,000*g* for 15 min) before being washed with sterile water and resuspended in 10 mL of YPGE (1% bacto-yeast extract, 2% bacto-peptone, 3% glycerol, and 3% ethanol). Bioconversions were initiated by feeding recombinant yeasts with 125 μM tabersonine during 24 h to yield lochnericine. Induction of T19H/TAT, T16H2/16OMT, or T19H/TAT/T16H2/TAT expression was then carried out during 16 to 24 h by the addition of sterile Gal (2%) to allow the syntheses of 19-acetylhörhammericine, lochnerinine, or 16-methoxy-19-acetylhörhammericine, which were analyzed as described by Carqueijeiro et al. (2018).

Accession Numbers

GenBank accession numbers are as follows: TEX1 (CYP1D521) and TEX2 (CYP71D347) are MG873080 and MG873081, respectively.

Supplemental Data

The following supplemental materials are available.

Supplemental Figure S1. Alignment of the amino acid sequences of tabersonine 6,7-epoxidase candidates.

Supplemental Figure S2. MS/MS spectra of the $[M+H]^+$ ion from CRO_T019212 and CRO_T013902 main reaction products.

Supplemental Figure S3. NMR data and key NOESY correlations for lochnericine.

Supplemental Figure S4. Steady-state Michaelis-Menten kinetics derived from initial rates of TEX1- or TEX2-enriched microsomes with tabersonine.

Supplemental Figure S5. Coexpression of T19H and TEX1 or TEX2 in yeast does not result in the synthesis of hörhammericine.

Supplemental Figure S6. Alignment of amino acid sequences of TEX1 and TEX2 and transmembrane helix prediction.

Supplemental Figure S7. Coexpression of TEX1, T16H2, 16OMT, T19H, and TAT in yeast led to the controlled synthesis of 16-methoxy-19-acetylhörhammericine from tabersonine.

Supplemental Figure S8. TEX 1 and TEX2 promoter analysis.

Supplemental Table S1. List of candidate genes identified through Spearman correlation analysis using T19H as a bait.

Supplemental Table S2. Correspondence between reconstituted transcripts and genes from the *C. roseus* genome.

Supplemental Table S3. Identity between the newly identified P450 candidate genes and T16H.

Supplemental Table S4. MIA quantification in main *C. roseus* organs.

Supplemental Table S5. Quantification of tabersonine- and lochnericine-type MIAs in *C. roseus* roots, adventitious roots, and hairy roots.

Supplemental Table S6. Primers used in this study.

ACKNOWLEDGMENTS

We thank Marie-Antoinette Marquet, Evelyne Danos, Emeline Marais, and Cédric Labarre (EA2106 Biomolécules et Biotechnologies Végétales) for help in maintaining cell cultures/plants and for valuable technical assistance. We also acknowledge the Fédération CaSciModOT for access to the computing grid. We thank Dr. David Nelson (University of Tennessee, Memphis) for CYP annotation.

Received May 8, 2018; accepted June 13, 2018; published June 22, 2018.

LITERATURE CITED

Besseau S, Kellner F, Lanoue A, Thamm AM, Salim V, Schneider B, Geu-Flores F, Höfer R, Guirimand G, Guihur A, (2013) A pair of tabersonine 16-hydroxylases initiates the synthesis of vindoline in an organ-dependent manner in *Catharanthus roseus*. Plant Physiol **163**: 1792–1803

Brown S, Clastre M, Courdavault V, O'Connor SE (2015) De novo production of the plant-derived alkaloid strictosidine in yeast. Proc Natl Acad Sci USA **112**: 3205–3210

Camacho C, Coulouris G, Avagyan V, Ma N, Papadopoulos J, Bealer K, Madden TL (2009) BLAST+: architecture and applications. BMC Bioinformatics **10**: 421

Caputi L, Franke J, Farrow SC, Chung K, Payne RME, Nguyen TD, Dang TTT, Soares Teto Carqueijeiro I, Koudounas K, Dugé de Bernonville T, Ameyaw B, Jones DM, et al. (2018) Missing enzymes in the biosynthesis of the anticancer drug vinblastine in Madagascar periwinkle. Science **360**: 1235–1239

Carqueijeiro I, Dugé de Bernonville T, Lanoue A, Dang TT, Teijaro CN, Paetz C, Billet K, Mosquera A, Oudin A, Besseau S, (2018) A BAHD acyltransferase catalyzing 19-O-acetylation of tabersonine derivatives in roots of *Catharanthus roseus* enables combinatorial synthesis of monoterpene indole alkaloids. Plant J **94**: 469–484

Courdavault V, Papon N, Clastre M, Giglioli-Guivarc'h N, St-Pierre B, Burlat V (2014) A look inside an alkaloid multisite plant: the Catharanthus logistics. Curr Opin Plant Biol **19**: 43–50

Dugé de Bernonville T, Clastre M, Besseau S, Oudin A, Burlat V, Glévarec G, Lanoue A, Papon N, Giglioli-Guivarc'h N, St-Pierre B, (2015a) Phytochemical genomics of the Madagascar periwinkle: unravelling the last twists of the alkaloid engine. Phytochemistry **113**: 9–23

Dugé de Bernonville T, Foureau E, Parage C, Lanoue A, Clastre M, Londono MA, Oudin A, Houillé B, Papon N, Besseau S, (2015b) Characterization of a second secologanin synthase isoform producing both secologanin and secoxyloganin allows enhanced de novo assembly of a *Catharanthus roseus* transcriptome. BMC Genomics **16**: 619

Dugé de Bernonville T, Carqueijeiro I, Lanoue A, Lafontaine F, Sánchez Bel P, Liesecke F, Musset K, Oudin A, Glévarec G, Pichon O, (2017) Folivory elicits a strong defense reaction in *Catharanthus roseus*: metabolomic and transcriptomic analyses reveal distinct local and systemic responses. Sci Rep **7**: 40453

Eddy SR (2011) Accelerated profile HMM searches. PLOS Comput Biol **7**: e1002195

Facchini PJ, De Luca V (2008) Opium poppy and Madagascar periwinkle: model non-model systems to investigate alkaloid biosynthesis in plants. Plant J **54**: 763–784

Farnsworth NR, Loub WD, Blomster RN, Abraham DJ (1968) Catharanthus alkaloids. 18. Isolation of hörhammerinine, a new alkaloid from *C. lanceus* (Apocynaceae). Z Naturforsch B **23**: 1061–1063

Feng T, Li Y, Wang YY, Cai XH, Liu YP, Luo XD (2010) Cytotoxic indole alkaloids from *Melodinus tenuicaudatus*. J Nat Prod **73**: 1075–1079

Fernández-Pérez F, Almagro L, Pedreño MA, Gómez Ros LV (2013) Synergistic and cytotoxic action of indole alkaloids produced from elicited cell cultures of *Catharanthus roseus*. Pharm Biol **51**: 304–310

Foureau E, Carqueijeiro I, Dugé de Bernonville T, Melin C, Lafontaine F, Besseau S, Lanoue A, Papon N, Oudin A, Glévarec G, (2016) Prequels to synthetic biology: from candidate gene identification and validation to enzyme subcellular localization in plant and yeast cells. Methods Enzymol **576**: 167–206

Geerlings A, Ibañez MM, Memelink J, van Der Heijden R, Verpoorte R (2000) Molecular cloning and analysis of strictosidine beta-D-glucosidase, an enzyme in terpenoid indole alkaloid biosynthesis in *Catharanthus roseus*. J Biol Chem **275**: 3051–3056

Giddings LA, Liscombe DK, Hamilton JP, Childs KL, DellaPenna D, Buell CR, O'Connor SE (2011) A stereoselective hydroxylation step of alkaloid

biosynthesis by a unique cytochrome P450 in *Catharanthus roseus*. J Biol Chem **286**: 16751–16757

Góngora-Castillo E, Childs KL, Fedewa G, Hamilton JP, Liscombe DK, Magallanes-Lundback M, Mandadi KK, Nims E, Runguphan W, Vaillancourt B, (2012) Development of transcriptomic resources for interrogating the biosynthesis of monoterpene indole alkaloids in medicinal plant species. PLoS ONE **7**: e52506

Gorman M, Neuss N, Svoboda GH, Barnes AJ Jr, Cone NJ (1959) A note on the alkaloids of Vinca rosea Linn. (*Catharanthus roseus* G. Don.). II. Catharanthine, lochnericine, vindolinine, and vindoline. J Am Pharm Assoc Am Pharm Assoc **48**: 256–257

Guirimand G, Burlat V, Oudin A, Lanoue A, St-Pierre B, Courdavault V (2009) Optimization of the transient transformation of *Catharanthus roseus* cells by particle bombardment and its application to the subcellular localization of hydroxymethylbutenyl 4-diphosphate synthase and geraniol 10-hydroxylase. Plant Cell Rep **28**: 1215–1234

Guirimand G, Courdavault V, Lanoue A, Mahroug S, Guihur A, Blanc N, Giglioli-Guivarc'h N, St-Pierre B, Burlat V (2010) Strictosidine activation in Apocynaceae: towards a "nuclear time bomb"? BMC Plant Biol **10**: 182

Heitz T, Widemann E, Lugan R, Miesch L, Ullmann P, Désaubry L, Holder E, Grausem B, Kandel S, Miesch M, (2012) Cytochromes P450 CYP94C1 and CYP94B3 catalyze two successive oxidation steps of plant hormone jasmonoyl-isoleucine for catabolic turnover. J Biol Chem **287**: 6296–6306

Kai T, Zhang L, Wang X, Jing A, Zhao B, Yu X, Zheng J, Zhou F (2015) Tabersonine inhibits amyloid fibril formation and cytotoxicity of Aβ(1-42). ACS Chem Neurosci **6**: 879–888

Kam TS, Pang HS, Lim TM (2003) Biologically active indole and bisindole alkaloids from Tabernaemontana divaricata. Org Biomol Chem **1**: 1292–1297

Kellner F, Geu-Flores F, Sherden NH, Brown S, Foureau E, Courdavault V, O'Connor SE (2015) Discovery of a P450-catalyzed step in vindoline biosynthesis: a link between the aspidosperma and eburnamine alkaloids. Chem Commun (Camb) **51**: 7626–7628

Kojima I, Umezawa K (2006) Conophylline: a novel differentiation inducer for pancreatic beta cells. Int J Biochem Cell Biol **38**: 923–930

Koroch ARH, Juliani R, Kulakowski D, Arthur H, Asante-Dartey J, Simon JE (2009) Voacanga africana: chemistry, quality and pharmacological activity. In HR Juliani, JE Simon, C-T Ho, eds, African Natural Plant Products: New Discoveries and Challenges in Chemistry and Quality. ACS Symposium Series 1021. American Chemical Society, Washington DC, pp 363-380

Laflamme P, St-Pierre B, De Luca V (2001) Molecular and biochemical analysis of a Madagascar periwinkle root-specific minovincinine-19-hydroxy-*O*-acetyltransferase. Plant Physiol **125**: 189–198

Leivar P, Quail PH (2011) PIFs: pivotal components in a cellular signaling hub. Trends Plant Sci **16**: 19–28

Levac D, Murata J, Kim WS, De Luca V (2008) Application of carborundum abrasion for investigating the leaf epidermis: molecular cloning of *Catharanthus roseus* 16-hydroxytabersonine-16-O-methyltransferase. Plant J **53**: 225–236

Lim KH, Hiraku O, Komiyama K, Kam TS (2008) Jerantinines A-G, cytotoxic Aspidosperma alkaloids from *Tabernaemontana corymbosa*. J Nat Prod **71**: 1591–1594

Liscombe DK, O'Connor SE (2011) A virus-induced gene silencing approach to understanding alkaloid metabolism in *Catharanthus roseus*. Phytochemistry **72**: 1969–1977

Luijendijk TJC, van der Meijden E, Verpoorte R (1996) Involvement of strictosidine as a defensive chemical in *Catharanthus roseus*. J Chem Ecol **22**: 1355–1366

Maloney EM, Farnsworth NR, Blomster RN, Abraham DJ, Sharkey AG Jr (1965) *Catharanthus lanceus*. VII. Isolation of tetrahydroalstonine, lochnerinine, and periformyline. J Pharm Sci **54**: 1166–1168

Marin E, Nussaume L, Quesada A, Gonneau M, Sotta B, Hugueney P, Frey A, Marion-Poll A (1996) Molecular identification of zeaxanthin epoxidase of Nicotiana plumbaginifolia, a gene involved in abscisic acid biosynthesis and corresponding to the ABA locus of *Arabidopsis thaliana*. EMBO J **15**: 2331–2342

Meisner J, Weissenberg M, Palevitch D, Aharonson N (1981) Phagodeterrency induced by leaves and leaf extracts of *Catharanthus roseus* in the larva of *Spodoptera littoralis*. J Econ Entomol **74**: 131–135

Miettinen K, Dong L, Navrot N, Schneider T, Burlat V, Pollier J, Woittiez L, van der Krol S, Lugan R, Ilc T, (2014) The seco-iridoid pathway from *Catharanthus roseus*. Nat Commun **5**: 3606

Nair CPN, Pillay PPP (1959) Lochnericine: a new alkaloid from *Lochnera rosea*. Tetrahedron **6**: 89–91

Nelson BK, Cai X, Nebenführ A (2007) A multicolored set of in vivo organelle markers for co-localization studies in Arabidopsis and other plants. Plant J **51**: 1126–1136

O'Connor SE, Maresh JJ (2006) Chemistry and biology of monoterpene indole alkaloid biosynthesis. Nat Prod Rep **23**: 532–547

Parage C, Foureau E, Kellner F, Burlat V, Mahroug S, Lanoue A, Dugé de Bernonville T, Londono MA, Carqueijeiro I, Oudin A, (2016) Class II cytochrome P450 reductase governs the biosynthesis of alkaloids. Plant Physiol **172**: 1563–1577

Patro R, Duggal G, Love MI, Irizarry RA, Kingsford C (2017) Salmon provides fast and bias-aware quantification of transcript expression. Nat Methods **14**: 417–419

Peebles CA, Shanks JV, San KY (2009) The role of the octadecanoid pathway in the production of terpenoid indole alkaloids in *Catharanthus roseus* hairy roots under normal and UV-B stress conditions. Biotechnol Bioeng **103**: 1248–1254

Pompon D, Louerat B, Bronine A, Urban P (1996) Yeast expression of animal and plant P450s in optimized redox environments. Methods Enzymol **272**: 51–64

Qu Y, Easson ML, Froese J, Simionescu R, Hudlicky T, De Luca V (2015) Completion of the seven-step pathway from tabersonine to the anticancer drug precursor vindoline and its assembly in yeast. Proc Natl Acad Sci USA **112**: 6224–6229

Qu Y, Easson MEAM, Simionescu R, Hajicek J, Thamm AMK, Salim V, De Luca V (2018) Solution of the multistep pathway for assembly of corynanthean, strychnos, iboga, and aspidosperma monoterpenoid indole alkaloids from 19*E*-geissoschizine. Proc Natl Acad Sci USA **115**: 3180–3185

Rasbery JM, Shan H, LeClair RJ, Norman M, Matsuda SP, Bartel B (2007) *Arabidopsis thaliana* squalene epoxidase 1 is essential for root and seed development. J Biol Chem **282**: 17002–17013

R Development Core Team (2013) R: A Language and Environment for Statistical Computing.R Foundation for Statistical Computing, Vienna

Rodriguez S, Compagnon V, Crouch NP, St-Pierre B, De Luca V (2003) Jasmonate-induced epoxidation of tabersonine by a cytochrome P-450 in hairy root cultures of *Catharanthus roseus*. Phytochemistry **64**: 401–409

Roepke J, Salim V, Wu M, Thamm AM, Murata J, Ploss K, Boland W, De Luca V (2010) Vinca drug components accumulate exclusively in leaf exudates of Madagascar periwinkle. Proc Natl Acad Sci USA **107**: 15287–15292

Schröder G, Unterbusch E, Kaltenbach M, Schmidt J, Strack D, De Luca V, Schröder J (1999) Light-induced cytochrome P450-dependent enzyme in indole alkaloid biosynthesis: tabersonine 16-hydroxylase. FEBS Lett **458**: 97–102

Sievers F, Wilm A, Dineen D, Gibson TJ, Karplus K, Li W, Lopez R, McWilliam H, Remmert M, Söding J, (2011) Fast, scalable generation of high-quality protein multiple sequence alignments using Clustal Omega. Mol Syst Biol **7**: 539

Stavrinides A, Tatsis EC, Foureau E, Caputi L, Kellner F, Courdavault V, O'Connor SE (2015) Unlocking the diversity of alkaloids in *Catharanthus roseus*: nuclear localization suggests metabolic channeling in secondary metabolism. Chem Biol **22**: 336–341

Stavrinides A, Tatsis EC, Caputi L, Foureau E, Stevenson CE, Lawson DM, Courdavault V, O'Connor SE (2016) Structural investigation of heteroyohimbine alkaloid synthesis reveals active site elements that control stereoselectivity. Nat Commun **7**: 12116

St-Pierre B, Laflamme P, Alarco AM, De Luca V (1998) The terminal O-acetyltransferase involved in vindoline biosynthesis defines a new class of proteins responsible for coenzyme A-dependent acyl transfer. Plant J **14**: 703–713

St-Pierre B, Besseau S, Clastre M, Courdavault V, Courtois M, Crèche J, Ducos E, Dugé de Bernonville T, Dutilleul C, Glévarec G, (2013) New light on alkaloid biosynthesis and future prospects. Adv Bot Res **68**: 73–109

Sun J, Ma L, San KY, Peebles CA (2017) Still stable after 11 years: a *Catharanthus roseus* hairy root line maintains inducible expression of anthranilate synthase. Biotechnol Prog **33**: 66–69

Sun J, Zhao L, Shao Z, Shanks J, Peebles CAM (2018) Expression of tabersonine 16-hydroxylase and 16-hydroxytabersonine-O-methyltransferase in *Catharanthus roseus* hairy roots. Biotechnol Bioeng **115**: 673–683

Sung YC, Lin CP, Chen JC (2014) Optimization of virus-induced gene silencing in *Catharanthus roseus*. Plant Pathol **63**: 1159–1167

Szabó LF (2008) Rigorous biogenetic network for a group of indole alkaloids derived from strictosidine. Molecules **13**: 1875–1896

Tatsis EC, Carqueijeiro I, Dugé de Bernonville T, Franke J, Dang TT, Oudin A, Lanoue A, Lafontaine F, Stavrinides AK, Clastre M, (2017) A three enzyme system to generate the Strychnos alkaloid scaffold from a central biosynthetic intermediate. Nat Commun **8**: 316

van der Heijden R, Jacobs DI, Snoeijer W, Hallard D, Verpoorte R (2004) The Catharanthus alkaloids: pharmacognosy and biotechnology. Curr Med Chem **11**: 607–628

Van Moerkercke A, Fabris M, Pollier J, Baart GJ, Rombauts S, Hasnain G, Rischer H, Memelink J, Oksman-Caldentey KM, Goossens A (2013) CathaCyc, a metabolic pathway database built from *Catharanthus roseus* RNA-Seq data. Plant Cell Physiol **54**: 673–685

Weaver J, Goklany S, Rizvi N, Cram EJ, Lee-Parsons CW (2014) Optimizing the transient Fast Agro-mediated Seedling Transformation (FAST) method in *Catharanthus roseus* seedlings. Plant Cell Rep **33**: 89–97

Westekemper P, Wieczorek U, Gueritte F, Langlois N, Langlois Y, Potier P, Zenk MH (1980) Radioimmunoassay for the determination of the indole alkaloid vindoline in Catharanthus. Planta Med **39**: 24–37

Xiao M, Zhang Y, Chen X, Lee EJ, Barber CJS, Chakrabarty R, Desgagné-Penix I, Haslam TM, Kim YB, Liu E, (2013) Transcriptome analysis based on next-generation sequencing of non-model plants producing specialized metabolites of biotechnological interest. J Biotechnol **166**: 122–134

Zhao S, Andrade RB (2013) Domino Michael/Mannich/N-alkylation route to the tetrahydrocarbazole framework of aspidosperma alkaloids: concise total syntheses of (−)-aspidospermidine, (−)-tabersonine, and (−)-vincadifformine. J Am Chem Soc **135**: 13334–13337